A Study of Wind Stress and Heat Flux over the Open Ocean by the Inertial-Dissipation Method

R. J. ANDERSON

Department of Fisheries and Oceans, Bedford Institute of Oceanography, Dartmouth, Nova Scotia, Canada

(Manuscript received 3 March 1992, in final form 16 October 1992)

ABSTRACT

A bow-mounted propeller anemometer and fast-response temperature sensors were operated during several cruises of CSS *Dawson*. Spectra of wind speed and temperature fluctuations were measured over the open ocean for a wind speed range of 6 to 21 m s^{-1} and a sea–air temperature difference range of ±6°C. Wind stress on the sea surface and sensible heat fluxes were determined by the inertial-dissipation method over a wide range of wind speeds for both stable and unstable atmospheric conditions. Neutral drag and sensible heat flux coefficients as functions of the wind speed at a 10-m reference height are in excellent agreement with the only existing eddy fluxes measured over the ocean from a stable platform and also with open sea inertial-dissipation measurements from a ship.

1. Introduction

In a wide range of oceanographic and marine meteorological studies it is desirable to have a measure of wind stress and heat flux at the sea surface but the logistics required to directly measure these parameters are too demanding for all but specialized studies. Most measurements have been taken at nearshore sites that can be influenced by shorelines, limited fetch, and shallow-water waves (e.g., Garratt 1977; Blanc 1985). The most direct method (eddy correlation) requires simultaneous measurements of vertical and horizontal wind fluctuations, and thus stable platforms or masts (e.g., Fletcher et al. 1985) are needed to avoid contamination of vertical wind fluctuations by flow distortion or sensor motion. The dataset of Smith (1980) is believed to be the only comprehensive eddy correlation study of wind stress in open ocean conditions.

Fluctuations of horizontal wind speed and temperature are less vulnerable to flow distortion and sensor motion errors and can be made from a mast at the bow of a ship facing into the wind. Large (1979) and Large and Pond (1981, 1982; henceforth LP) reported wind stress and sensible heat flux estimates over the open ocean using an inertial-dissipation method to infer the wind stress and heat flux from measurements of wind speed and temperature fluctuations. The advantage of this method is that the required measurements are much simpler. To infer surface fluxes from wind and temperature spectra, a chain of theoretical relations invoking the inertial subrange, local isotropy, and vertical transfer of turbulent energy is required (e.g., Fairall and Larsen 1986). Several slightly different formulas have been used in the past. Large (1979) and LP made eddy correlation measurements from a specially designed moored stable platform (Smith 1980) and chose a set of "dissipation" formulas that gave general agreement with their direct eddy correlation results for the same dataset. They then used a much larger set of dissipation data from ships to derive bulk formulas for estimation of wind stress and heat flux over a wider range of wind speeds, air temperatures, and sea surface temperatures. Their results may be viewed as an extrapolation of the eddy correlation measurements against which they calibrated their formulas.

Since formulas used in various "inertial dissipation" studies have had minor differences, their results are still often viewed as unconfirmed. Dissipation data taken from a bow mast during seven cruises of CSS *Dawson*, analyzed by the same methods used by LP, give similar bulk relations for the dependence of the neutral drag coefficient, C_{10N}, and heat flux coefficient, C_{TN}, on wind speed. Cruise locations ranged from Georges Bank to the Labrador Sea, and water depth exceeded 70 m in all cases.

2. Method

The formulas and coefficients used by LP will be used in this paper. In the theory of isotropic turbulence it is argued that there is an inertial subrange of frequencies where a cascade of turbulent energy between a source region (lower frequencies) and a dissipation

Corresponding author address: Dr. Robert J. Anderson, Department of Fisheries and Oceans, Bedford Institute of Oceanography, Dartmouth, Nova Scotia, B2Y 4A2, Canada.

region (higher frequencies) is characterized by a power spectrum of the form

$$\Phi_1(f) = \alpha_u \epsilon^{2/3} (U/2\pi)^{2/3} f^{-5/3}, \quad (1)$$

and, assuming isotropy

$$\Phi_2(f) = \Phi_3(f) = \frac{4}{3}\Phi_1(f), \quad (2)$$

where Φ_1 is a downwind spectral value at frequency f, and Φ_2 and Φ_3 are crosswind and vertical spectral values, respectively. The factor $(U/2\pi)$ arises from the frozen turbulence (Taylor's) hypothesis to convert wavenumber to frequency. The rate of viscous dissipation of kinetic energy is ϵ and $\alpha_u = 0.55$ is the Kolmogorov constant.

The temperature spectrum is

$$\Phi_t(f) = \beta_T N_T \epsilon^{-1/3} (U/2\pi)^{2/3} f^{-5/3}, \quad (3)$$

where $\beta_T = 0.80$ is the Kolmogorov constant for temperature and N_T is the diffusive dissipation rate of the temperature variance.

From a comparison of their eddy flux and dissipation data, LP inferred that the vertical divergence of kinetic energy flux can be neglected and found that from several alternatives the best agreement with eddy fluxes was given by

$$u_*^2 = (kz\epsilon)^{2/3} [\phi_m(z/L) - z/L]^{-2/3}, \quad (4)$$

where u_* is the friction velocity, z is the measurement height, $k = 0.4$ is the von Kármán constant, L is the Monin–Obukov length (defined below) and the dimensionless vertical gradient of the mean wind speed, $\phi_m(z/L)$, is a function of atmospheric stability. This is the formulation used by Khalsa and Businger (1977) and Anderson (1987). Similar formulations are used to estimate temperature (and also humidity) fluxes from their respective power spectra (LP; Smith and Anderson 1984; Andreas 1987):

$$\overline{tu}_3 = [ku_* N_T z]^{1/2} [\phi_t(z/L)]^{-1/2}, \quad (5)$$

where N_T is obtained from (3), u_* is derived from (4), and $\phi_t(z/L)$ is the dimensionless vertical temperature gradient. The atmospheric stability is

$$z/L = -gkz\overline{t_v u}_3 / T_v u_*^3, \quad (6)$$

where g is acceleration due to gravity and T_v (with fluctuation t_v) is the virtual temperature or the temperature of dry air, which would have the same density as air with temperature T and water vapor density ρ_v. The dimensionless gradient terms in (4) and (5) used by LP (1982) are

$$\phi_m(z/L) = \phi_t(z/L) = 1 + 7z/L \quad \text{stable}, \quad z/L \geq 0 \quad (7)$$

$$\phi_m(z/L) = (1 - 16z/L)^{-1/4} \quad \text{unstable}, \quad z/L < 0 \quad (8)$$

$$\phi_t(z/L) = (1 - 16z/L)^{-1/2} \quad \text{unstable}, \quad z/L < 0. \quad (9)$$

The forms are those recommended by Dyer (1974) in his review of flux profile relationships, but a 40% stronger z/L dependence is used in stable conditions (see Wieringa 1980; Edson et al. 1991).

The profile of mean wind speed is given by

$$U = (u_*/k)[\ln z/z_0 - \psi_m], \quad (10)$$

where z_0 is a roughness length and ψ_m is the integrated flux gradient relationship for momentum, which for stable cases $(z/L > 0)$ is

$$\psi_m = \psi_t = -7z/L \quad (11)$$

and is equal to the relationship for temperature, ψ_t, and for unstable cases $(z/L < 0)$, as derived by Paulson (1970), is

$$\psi_m = 2\ln[(1+x)/2] + \ln[(1+x^2)/2] - 2\tan^{-1}x + \pi/2, \quad (12)$$

$$\psi_t = 2\ln[(1+x^2)/2], \quad (13)$$

where $x^4 = 1 - 16z/L$. By solving (10) for the roughness length, an equivalent neutral drag coefficient

$$C_{10N} = k^2/[\ln(10/z_0)]^2 \quad (14)$$

and a neutral 10-m wind speed

$$U_{10N} = u_* \ln(10/z_0)/k \quad (15)$$

can be found in order to eliminate stability dependence.

The neutral heat flux coefficient at 10 m is

$$C_{TN} = k^2/[\ln(10/z_0)\ln(10/z_{0t})], \quad (16)$$

where z_{0t} is a thermal roughness length derived from the bulk temperature difference

$$T_z - T_s = t_*[\ln(z/z_{0t}) - \psi_t], \quad (17)$$

and the scaling temperature is $t_* = -\overline{tu}_3/ku_*$.

3. Instrumentation

A Gill propeller–vane anemometer (R. M. Young Co.) with an extended vertical shaft and a four-bladed 19-cm polystyrene propeller was used to measure wind speed and direction. This instrument uses a simple dc generator for wind speed and a resistance potentiometer for direction. It is very reliable and has a linear calibration, which is stable. The base has been modified to incorporate a fast-response temperature probe. The

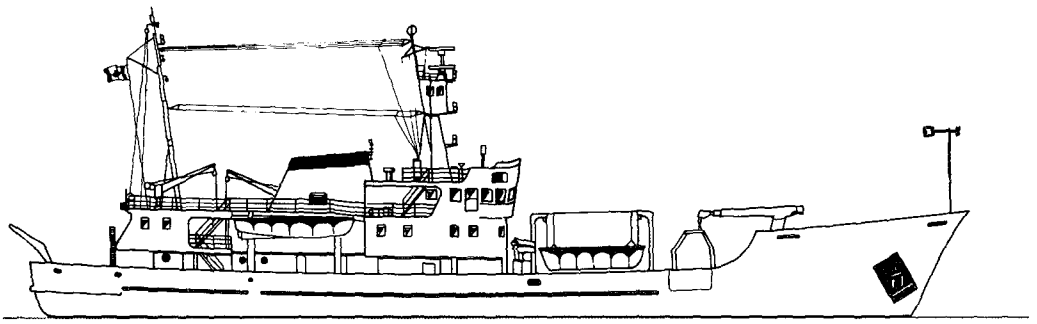

FIG. 1. CSS *Dawson*, showing the placement of the bow mast. The vessel is 64.5 m in length.

fine microbead thermistor is hermetically sealed in a thin glass coating and fastened in a mount by two fine wires. The probe is shielded from solar radiation by a small hat. This sensor package was mounted at 12.5 m above mean sea level on an aluminum mast fixed over the ship's bow (Fig. 1). Subsequent field tests (to be reported separately) and wind tunnel tests (Thiébaux 1990) indicate negligible flow distortion at this height for bow-on winds (±45°). Mean air temperatures from the bow mast thermistors were compared with psychrometer readings taken from the ship's bridge and also with a mercury thermometer at deck level. Sea temperatures were obtained from one of three sources: bucket thermometer readings by the ship's officers, engine cooling water intake from a dial readout, and CTD data whenever the CTD package was resting just below the surface. Because of discrepancies among these temperatures, data from a sea temperature probe at −1.0 m and a second air temperature probe on the bow mast were logged during the cruises in 1988.

These identical temperature probes (FASTIP) consist of a small microbead thermistor encased in the tip of a thin glass rod. According to the manufacturer's specifications, the FASTIP has similar response characteristics to the microbead in still air but can also be used and easily calibrated in water.

4. Data recording and analysis

Wind speed, direction relative to the ship's heading, and fast temperature signals were low-pass filtered at 8 Hz and recorded in serial digital format at 16 samples per second on audio cassettes and on 9-track tapes by the ship's minicomputer. During data recording the ship was held on station with the bow into the wind. Duration of the data runs varied from 7 to 40 minutes with most being in excess of 20 minutes. Data were analyzed at the Bedford Institute of Oceanography using a Cyber mainframe computer. Calibrations were applied, means and linear trends were calculated and removed, and spectral analysis was performed in blocks of 2048 samples. A hanning window was applied to each block. The spectral estimates were averaged in 23 logarithmically spaced frequency bands between 0.005 and 8 Hz. (LP, with limited data storage in the field, only looked at three filtered frequencies around 1 Hz.)

Frequency response of the Gill anemometer is limited by the amount of passing air needed to spin up the propeller. The propeller is assumed to have an RC filter behavior in the form $2\pi f_0 = U/D$, where f_0 is the filter frequency, U is the mean wind speed, and a distance constant, $D = 1.0$ m for the propellers used, is the wind passage required for a 63% recovery from a step change in wind speed. A spectral correction array is applied to extend the usable part of the inertial subrange of the wind spectrum. The spectral density in each frequency band is multiplied by an amplitude correction, $[1 + (2\pi f_i D/U)^2]$, where f_i is the central

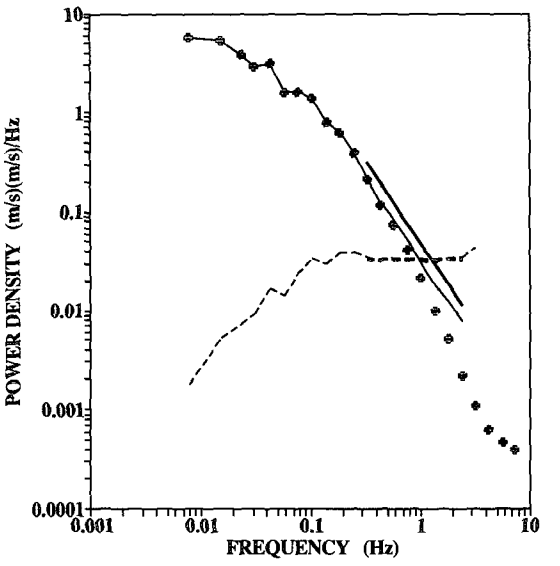

FIG. 2. Wind spectra before and after correction for frequency response of the Gill propeller-vane anemometer: (plus signs) raw spectral values, (thin solid line) corrected spectrum, (thick solid line) $f^{-5/3}$ slope, and (broken line) $f^{5/3}\Phi_1(f)$ (bold where the value is constant.) The wind speed for this run was 9.4 m s^{-1} and $\Delta T = -6.1$°C.

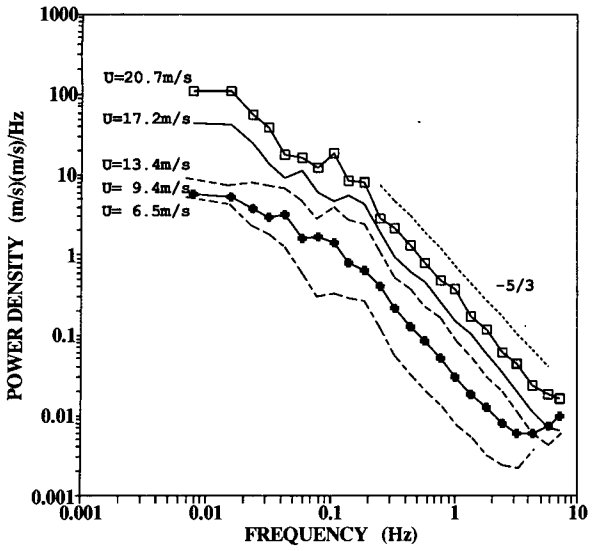

FIG. 3. Wind spectra for various wind speeds between 6.5 and 20.7 m s^{-1}. $\cdots, f^{-5/3}$ slope.

frequency of the band. Large and Pond used different, heavier propellers and made their distance constant a function of wind speed. Figure 2 shows wind spectra before and after correction. It also shows $f^{5/3}\Phi_1(f)$, which has a constant value for frequencies in the inertial subrange. The highest-frequency values in the raw spectrum are somewhat noisy, causing an increase in the corrected spectrum at the highest frequencies.

Examination of many wind spectra (Fig. 3) showed that the portion of the spectrum with constant $f^{5/3}\Phi_1(f)$ typically occurs above 0.35 Hz, which is above the frequency of dominant waves or ship's motion. (There is often a wave-frequency peak in the downwind spectrum.) This lower limit scarcely varied with wind speeds between 7 and 20 m s^{-1} or with atmospheric stability, and appears to be determined more by structure of the boundary layer than by surface-level scaling. The upper frequency limit is imposed mainly by the weight and diameter of the propeller, and by noise, which limits the rolloff compensation. The practical upper frequency limit is typically found to be about 2.5 Hz. Downwind spectral values averaged over four of the logarithmic frequency bands, usually between 0.6 and 2 Hz, provided the input for the dissipation formulas. A data run was rejected if the standard deviation of $f^{5/3}\Phi_1(f)$ in the four bands was greater than 10% of the mean.

An expansion of t_v in (6) gives the stability as

$$z/L = -gkz[\overline{tu}_3/T + 0.00047T\overline{\rho_v u}_3/T_k]/u_*^3, \quad (18)$$

where $T_k = 273.16°$ and $T = T_z + T_k$, and $\overline{\rho_v u}_3$ is the flux of absolute humidity and $\overline{tu}_3$ is the sensible heat flux. These flux terms can be estimated from bulk formulas, $\overline{tu}_3 = C_T U_z(T_s - T_z)$ and $\overline{\rho_v u}_3 = C_E U_z \Delta Q$, where C_T and C_E are sensible and latent heat flux coefficients. The absolute humidity difference between saturated air at T_s and air at T_z as used by LP is $\Delta Q = 0.98Q_{satsea} - \mathrm{RH}Q_{satair}$, and RH = 75% relative humidity has been assumed for T_z unless measured otherwise. Here C_E is assumed to be $1.2C_T$ in agreement with recent findings. Smith (1981, 1988) tabulated sea surface drag coefficients and heat flux coefficients over the sea as functions of wind speed and sea–air temperature difference for a number of measurement heights. The results presented here use the spectral values and means and the non-neutral heat flux coefficients, (Smith 1988), as initial inputs to Eqs. (1)–(18) [not (2) or (6)], in an iteration routine to establish u_* and z/L. The neutral drag coefficient, wind speed, and the sensible heat flux coefficient referenced to 10 m are then calculated.

5. Results and discussion

a. Mean wind speed

During two cruises in 1988, tests were made to confirm that the bow anemometer wind speeds were representative of open ocean conditions and relatively free of flow distortion from the ship. Comparisons were made between a R. M. Young wind monitor mounted on a MINIMET data buoy (Coastal Climate Co.) and the ship's bow and masthead anemometers while the ship was at anchor or on station within 800 m of the buoy. The comparisons are based on 10-min averages recorded on different logging systems. Sources of error include sensor separation, ship draft when not at anchor, possible differing start times due to differing log-

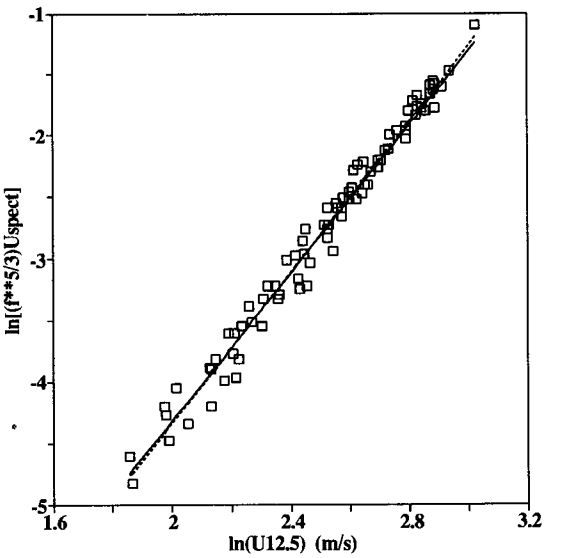

FIG. 4. Relationship between the measured power density in the inertial subrange, $f^{5/3}\Phi_1(f)$, and the measured wind speed: (solid line) regression line, (dotted line) cubic fit.

TABLE 1. Range of conditions for this study. Sites—SS: Scotian Shelf, LS: Labrador Shelf, GB: Georges Bank.

Cruise (year—number)	Month	Site	Runs	Wind speed range (m s^{-1})	($T_s - T_z$) range (°C)	z/L range
82—043	Dec	SS	21	6.5–15.2	−3.5–3.5	−0.24–0.11
83—018	Jun	LS	16	7.5–15.4	−6.1 – −1.1	0.02–1.25
83—032	Oct	SS	12	6.8–20.7	0.0–5.8	−1.12–0.00
83—034	Nov	GB	10	10.0–18.0	0.0–2.7	−0.10–0.00
88—023	Jun	GB	6	6.4–9.2	−3.1–0.9	−0.09–0.41
88—036	Oct	GB	13	9.1–17.9	−1.4–5.0	−0.06–0.15
88—040	Nov	SS	7	12.5–16.8	−1.1–0.0	0.00–0.04

ging clocks, and also the factors used to correct the wind profile up or down to 10-m elevation (atmospheric stability effects are more important at lower wind speeds). Wind speed data from the MINIMET anemometer at 3.0-m height were adjusted to 12.5-m height (Smith 1988) using the air–sea temperature differences from the buoy and were compared to the bow anemometer measurements. The bow anemometer wind speeds were also adjusted down to 3.0-m height and compared to the MINIMET winds as a separate comparison. There was agreement to within 1% for wind speeds above 14 m s^{-1} and to within 3% for lesser wind speeds.

Figure 4 compares the wind speed measured at a height of 12.5 m above mean water level (corrected for ship speed and tidal currents) with the spectral value in the inertial subrange. A regression line (solid) fits the data remarkably well,

$$\ln(f^{5/3}\Phi_1(f)) = -10.45 + 3.05 \ln U_z, \quad (19)$$

with correlation coefficient $r = 0.99$ for $n = 85$ points and does not differ significantly from a fitted cubic relationship (dashed line):

$$\ln(f^{5/3}\Phi_1(f)) = -10.32 + 3.0 \ln U_z,$$
$$f^{5/3}\Phi_1(f) = 3.3 \times 10^{-5} U_z^3. \quad (20)$$

b. *Wind stress*

A dataset of 85 runs from seven cruises is used. Other data were logged but were rejected because of low wind speeds (<6 m s^{-1}), noisy spectra in the inertial subrange, or relative wind directions beyond ±45 degrees of the bow. The ranges of wind speed and sea–air temperature differences for each cruise are shown in Table 1.

c. *Dependence of the drag coefficient on wind speed*

The neutral 10-m drag coefficient increases with the 10-m wind speed (Fig. 5a). The rate of increase de-

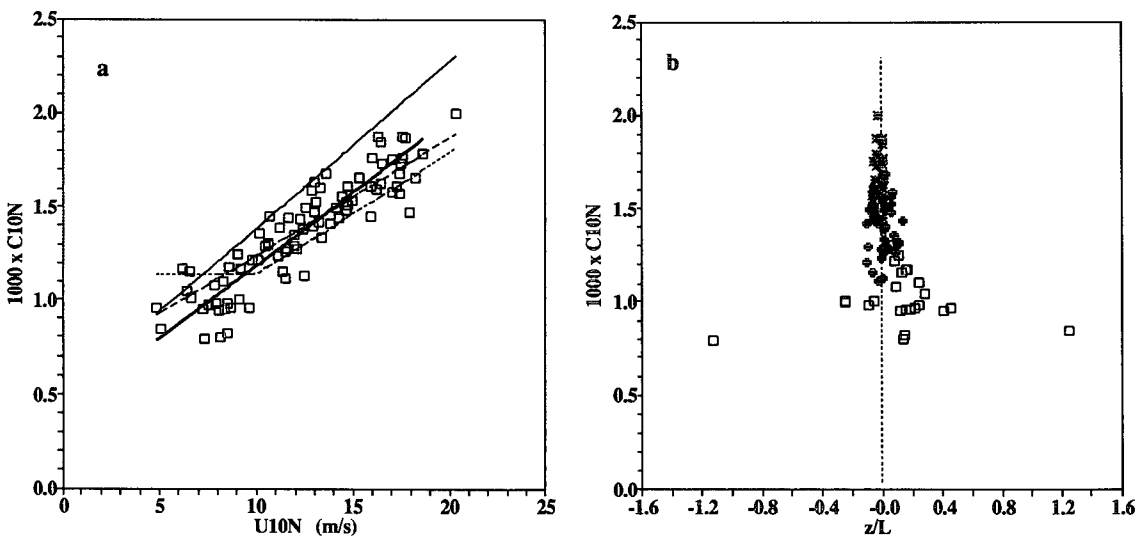

FIG. 5. (a) Plot of $10^3 C_{10N}$ vs U_{10N} with regression lines from Smith (1980) (dashed), LP (1981) (dotted), Smith et al. (1992) (thin solid), and this dataset (thick solid). (b) Plot of $10^3 C_{10N}$ vs stability for various wind speed ranges: (open square) $5 < U_{10N} < 10$ m s^{-1}, (plus sign) $10 < U_{10N} < 15$ m s^{-1}, and (asterisk) $15 < U_{10N}$ m s^{-1}.

pends on how a regression of drag coefficient on wind speed is fitted. If percent errors in both parameters are comparable it is appropriate to fit a "neutral" regression line, which is an average of regression lines with each parameter in turn as the independent variable. A neutral regression for all data from $4.5 < U_{10N} < 21$ m s^{-1} in this set,

$$10^3 C_{10N} = 0.40 + 0.079 U_{10N}, \qquad (21)$$

with correlation coefficient of 0.91 for 84 data points (highest point excluded) can be taken as the result of this study. (Compared to the one-way regression, the "neutral" regression has a higher slope by a factor $1/r$.)

Substitution of (20) in (1) and (4) would result in a relation between u_* and U_Z that would give the drag coefficient a slightly nonlinear dependence on wind speed. This would result in a similar range of drag coefficients as in Fig. 5a for $5 < U_{10N} < 10$ m s^{-1} but less variability for $U_{10N} > 15$ m s^{-1} than the data used to derive (21). The U_z exponent in (20) is quite sensitive to adding or deleting a small number of data points at high wind speeds and thus (20) is not recommended to estimate the spectral level in the inertial subrange and hence to estimate the neutral drag coefficient.

Comparison with earlier results:

Several options are explored in Table 2, which also includes the one-way regression lines from LP (1981), Smith (1980), and Smith et al. (1992) for comparison. The 61 drag coefficients with $10 < U_{10N} < 21$ m s^{-1} were regressed against U_{10N} to give

$$10^3 C_{10N} = 0.59 + 0.065 U_{10N}, \qquad (22)$$

with correlation coefficient 0.83. This is in excellent agreement with the lines of Smith (1980) and with LP (1981) for $U_{10N} > 10$ m s^{-1}.

Unlike LP (1981), there is no break in the variation of the drag coefficient at wind speeds < 10 m s^{-1}; the slope of the neutral regression line (Table 2) is not reduced by including drag coefficients over the entire range of wind speeds, $4.5 < U_{10N} < 21$ m s^{-1}.

TABLE 2. Regressions of drag coefficient on wind speed.

Data source	U_{10N} (m s^{-1})	Number of runs	Regression ($10^3 C_{10N}$ =)	Correlation coefficient r
This study	4.5–21	84	$0.49 + 0.071 U_{10N}$	0.91
Neutral			$0.40 + 0.079 U_{10N}$	0.91
	10–21	61	$0.59 + 0.065 U_{10N}$	0.83
Neutral			$0.39 + 0.080 U_{10N}$	0.83
Smith (1980)	6–22	63	$0.61 + 0.063 U_{10N}$	0.70
Large and Pond	4–10	618	1.14	
(1981)	10–26	973	$0.49 + 0.065 U_{10N}$	0.74
Garratt (1977)	3–21	791	$0.75 + 0.067 U_{10}$	
Smith et al. (1992)	4–20	330	$0.50 + 0.089 U_{10N}$	0.67

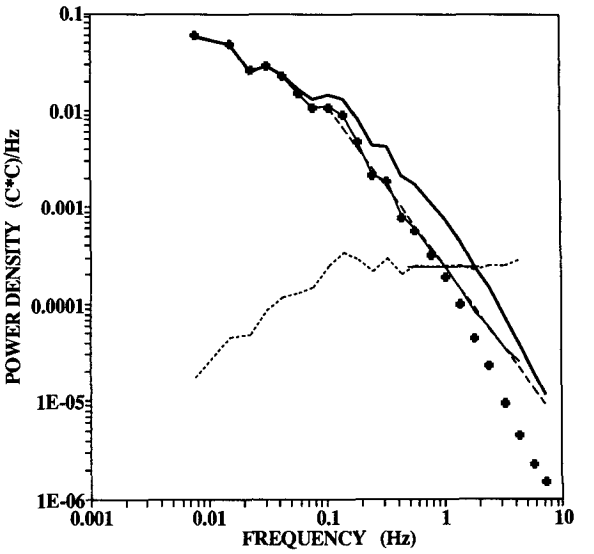

FIG. 6. Simultaneous temperature spectra for a FASTIP thermoprobe (+) and for a microbead thermistor probe (thick line), $f^{-5/3}$ slope (dashed line), FASTIP with a time constant correction applied (thin line), and $f^{5/3}\Phi_T(f)$ for the corrected Fastip (dotted line); the horizontal line is constant.

The line of Smith et al. (1992) is for inertial-dissipation analysis by K. L. Davidson of data taken from a ship in the southeastern North Sea during HEXMAX. Water depth was 30 m and waves tended to be less fully developed in this area than in the open North Atlantic, resulting in steeper waves and slightly higher drag coefficients. Davidson used $k = 0.35$ and $\alpha_u = 0.52$ in his analysis; his drag coefficients would increase by 3% if the constants were as used in this study.

Large and Businger (1988) reported inertial-dissipation drag coefficients from FASINEX at an offshore site. These generally supported LP (1981) but larger scatter of individual values may be associated with variability in the vicinity of an ocean SST front.

Figure 5b shows the neutral drag coefficient as a function of stability for various wind speed ranges. Higher values of the neutral drag coefficient are associated with stronger winds. In the two higher wind speed ranges the stability is always near neutral as a consequence of the u_*^{-3} dependence of z/L (mechanical turbulence dominates); in these cases the influence of stratification on the wind profile is small. The widest range of stability occurs for lowest wind speed range (5–10 m s^{-1}), and the flux gradient formulas using $7z/L$ for stable conditions [Eq. (7), (10)] make C_{10N} independent of stability (similar drag coefficients to those for unstable conditions at the same wind speeds) as expected, while a commonly used value of $5z/L$ (Dyer 1974) would have given higher values for stable

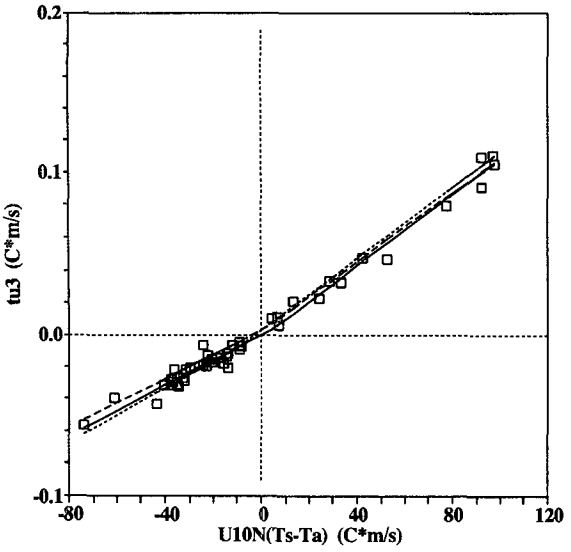

FIG. 7. Dissipation estimates of $\overline{tu}_3$ vs $U_{10N}(T_s - T_a)$ with neutral regression lines for stable and unstable conditions (solid). Regression lines from Smith (1980) (dotted line) and LP (1981) (dashed line) are included for comparison. Equations are listed in Table 3.

stratification than for unstable. The mean C_{10N} in this range is $(1.018 \pm 0.137) \times 10^{-3}$ for 24 data runs.

It should be mentioned that LP (1981) used $5z/L$ to calculate dissipation momentum fluxes for stable conditions, but it is noted in LP (1981) and in LP (1982) that $7z/L$ gave better agreement with Reynolds fluxes for $z/L > 0.1$.

d. *Heat flux*

Concurrent temperature spectra (Fig. 6) for two sensors, a "FASTIP" glass-coated thermistor bead and a microbead thermistor, show $f^{-5/3}$ regions. The microbead thermistor, with more variance at higher frequencies, has nearly three times the spectral level of the "FASTIP" probe. Mean temperatures from both thermistors were within 0.1°C for this 40-min data run. It is believed that in this particular run the microbead is contaminated by salty deposits and is responding to latent heat exchange as water condenses and evaporates from the salt in response to humidity fluctuations (Schmitt et al. 1978). Subsequent tests have shown that the FASTIP probes have an inherent gradual response roll-off. A time constant correction of 0.035 s, when applied to the FASTIP measured spectrum, gives the corrected fit in Fig. 6. Both types of spectral distortion can be difficult to detect and have a very important effect on heat flux measurements by eddy correlation and estimates from inertial dissipation. This is especially true if the entire temperature spectrum is not observed, as in the case when filters are used to obtain $f^{5/3}\Phi_t$ in only a few frequency bands.

Careful screening of the temperature data was required in order to obtain both valid spectra and reliable mean air and sea temperatures simultaneously. In many cases good temperature spectra accompanied by missing or suspect sea temperatures had to be rejected. Likewise, temperature spectra that displayed symptoms of salt contamination (distorted spectral shape) or were noisy due to spray, rain, or electrical interference were also rejected.

Figure 7 shows dissipation estimates of heat flux, $\overline{tu}_3$, plotted against $U_{10N}(T_{\text{Sea}} - T_z)$ with "neutral" (two-way) regression lines for stable and unstable conditions. Both these regressions are in agreement with earlier results of Smith (1980) and LP (1982) (Table 3). Data included in the plot were excluded from the regression analysis if $|\Delta T| < 1$°C, because of uncertainties in temperature data, or if $U_{10N}|\Delta T| < 10$°C m s^{-1} because of the uncertainties in correcting the wind profile during light wind conditions.

The neutral heat flux coefficient C_{TN} is much less dependent on wind speed U_{10N} than the drag coefficient (Fig. 8a). Within the scatter, these data do not resolve whether C_{TN} is independent of wind speed (as suggested by Smith 1980) or z_{0t} is independent of wind speed (LP 1982), giving a slight increase of C_{TN} with wind speed.

The neutral heat flux coefficient (Fig. 8b) shows no significant difference between the stable and unstable cases, indicating that the flux-gradient formulas [Eqs. (7–13) and (16)] are successful in accounting for the dependence of the heat flux on stability. Much of the heat flux data lies in the near-neutral region ($-0.2 < z/L < 0.2$) where stability has a small influence but

TABLE 3. Regression lines of heat flux on bulk parameters.

Data source	Condition	Number of runs	Regression equation $10^3\overline{tu}_3$ (°C m s^{-1})	Correlation coefficient r
This study	Stable	30	$-0.00 + 0.79(T_s - T_z)U_{10N}$	0.91
	Unstable	11	$-1.62 + 1.11(T_s - T_z)U_{10N}$	0.98
Smith (1980)	Stable	39	$-0.1 + 0.83(T_s - T_z)U_{10N}$	0.98
	Unstable	32	$3.2 + 1.10(T_s - T_z)U_{10N}$	0.97
Large and Pond (1982)	Stable	124	$2.3 + 0.74(T_s - T_z)U_{10N}$	0.89
	Unstable	179	$2.7 + 1.06(T_s - T_z)U_{10N}$	0.94

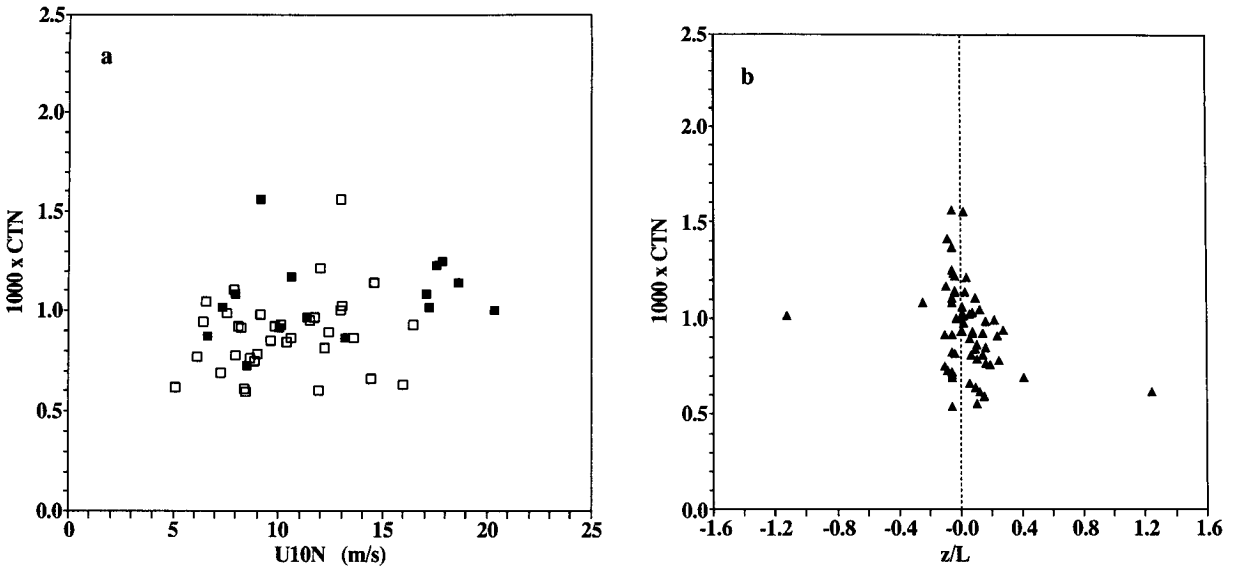

FIG. 8. (a) Neutral heat flux coefficient versus neutral wind speed at 10 m: (open squares) stable atmospheric conditions and (solid squares) unstable. (b) Neutral heat flux coefficient as a function of atmospheric stability.

heat flux coefficients for data outside this region, for generally lower wind speeds and larger sea–air temperature differences, were within the same range. Large and Pond (1982), with a much larger dataset, showed a significant difference between stable and unstable cases.

6. Conclusions

- This dataset confirms the dissipation results of LP and agrees with the eddy correlation results of Smith (1980) from a stable platform, thereby confirming values of the sea surface drag coefficients away from coastal and shallow water influences. Adjustments for sensor height and the influence of stratification are required.
- The inertial-dissipation technique, using robust and inexpensive sensors, gives reliable values for fluxes of momentum and heat from shipboard measurements in open ocean conditions. As a result of this study, the Bedford Institute has designed and built an automated, PC-based system for logging and analyzing inertial-dissipation data onboard ship.
- Flux gradient formulas using $7z/L$ in (11) for stable conditions account for the influence of stability on the wind and temperature profiles.
- Many temperature spectra were rejected because they were found to be influenced by salt contamination of the thermistor probes; this required careful screening of the data. Care must be taken to ensure that accurate temperature measurements are made and that the entire air temperature power spectrum is studied for reliability. In the future, steps will be taken to alleviate this problem by washing and if necessary replacing the probes. Redundancy in air temperature probes and use of a system to rinse contaminants from their surfaces are recommended.

Acknowledgments. I thank S. D. Smith and F. W. Dobson for their helpful comments on this manuscript. I also thank the senior scientists and ship's personnel who provided the opportunity and assistance to collect data on the various cruises, and D. L. Hendsbee for technical support.

REFERENCES

Anderson, R. J., 1987: Wind stress measurements over rough ice during the 1984 Marginal Ice Experiment. *J. Geophys. Res.*, **92**(C7), 6933–6941.

Andreas, E. L., 1987: Spectral measurements in a disturbed boundary layer over snow. *J. Atmos. Sci.*, **44**, 1912–1939.

Blanc, T. V., 1985: Variation of bulk-derived surface flux, stability and roughness results due to the use of different transfer coefficient schemes. *J. Phys. Oceanogr.*, **15**, 650–669.

Dyer, A. J., 1974: A review of flux-profile relationships. *Bound.-Layer Meteor.*, **7**, 363–372.

Edson, J. B., C. W. Fairall, P. G. Mestayer, and S. E. Larsen, 1991: A study of the inertial-dissipation method for computing air-sea fluxes. *J. Geophys. Res.*, **96**(C6), 10 689–10 711.

Fairall, C. W., and S. E. Larsen, 1986: Inertial dissipation methods and turbulent fluxes at the air-ocean interface. *Bound.-Layer Meteor.*, **34**, 287–301.

Fletcher, J., R. G. Mills, and S. D. Smith, 1985: Design, construction and performance of a moored stable platform. Canadian Tech. Rep. of Hydrography and Ocean Sciences, No. 62, Department of Fisheries and Oceans, Bedford Institute of Oceanography, Dartmouth, N.S., Canada, 41 pp.

Garratt, J. R., 1977: Review of drag coefficients over oceans and continents. *Mon. Wea. Rev.*, **105**, 915–929.

Khalsa, S., and J. A. Businger, 1977: The drag coefficient as deter-

mined by the dissipation method and it's relation to intermittent convection in the surface layer. *Bound.-Layer. Meteor.*, **12**, 273–297.

Large, W. G., 1979: The turbulent fluxes of momentum and sensible heat over the open ocean during moderate to strong winds. Ph.D. thesis, University of British Columbia, 180 pp.

——, and S. Pond, 1981: Open ocean momentum fluxes in moderate to strong winds. *J. Phys. Oceanogr.*, **11**, 324–336.

——, and ——, 1982: Sensible and latent heat flux measurements over the ocean. *J. Phys. Oceanogr.*, **12**, 464–482.

——, and J. A. Businger, 1988: A system for remote measurements of the wind stress over the ocean. *J. Atmos. Oceanic Technol.*, **5**, 274–284.

Paulson, C. A., 1970: Representation of wind speed and temperature profiles in the unstable surface layer. *J. Appl. Meteor.*, **9**, 857–861.

Schmitt, K. F., C. A. Friehe, and C. H. Gibson, 1978: Humidity sensitivity of atmospheric temperature sensors by salt contamination. *J. Phys. Oceanogr.*, **8**, 151–161.

Smith, S. D., 1980: Wind stress and heat flux over the ocean in gale force winds. *J. Phys. Oceanogr.*, **10**, 709–726.

——, 1981: Coefficients for sea-surface wind stress and heat exchange. Tech. Rep. BI-R-81-19, Bedford Institute of Oceanography, Dartmouth N.S., Canada, 31 pp.

——, 1988: Coefficients for sea surface wind stress, heat flux, and wind profiles as a function of wind speed and temperature. *J. Geophys. Res.*, **93**(C12), 467–472.

——, and R. J. Anderson, 1984: Spectra of humidity, temperature and wind over the sea at Sable Island, Nova Scotia. *J. Geophys. Res.*, **89**(C2), 2029–2040.

——, ——, W. A. Oost, C. Kraan, N. Maat, J. DeCosmo, K. Katsaros, K. L. Davidson, K. Bumke, L. Hasse, and H. M. Chadwick, 1992: Sea surface wind stress and drag coefficients. The HEXOS results. *Bound.-Layer. Meteor.*, **60**, 109–142.

Thiébaux, M. L., 1990: Wind tunnel experiments to determine correction functions for shipboard anemometers. Canadian Contractor Report of Hydrography and Ocean Sciences, No. 36, Department of Fisheries and Oceans, Bedford Institute of Oceanography, Dartmouth N.S., Canada, 57 pp.

Wieringa, J., 1980: A reevaluation of the Kansas mast influence on measurements of stress and cup anemometer overspeeding. *Bound.-Layer. Meteor.*, **18**, 411–430.